

pubs.acs.org/est Article

Redox Properties of Pyrogenic Dissolved Organic Matter (pyDOM) from Biomass-Derived Chars

Wenqing Xu,* Nicolas Walpen, Marco Keiluweit, Markus Kleber, and Michael Sander



Cite This: Environ. Sci. Technol. 2021, 55, 11434-11444



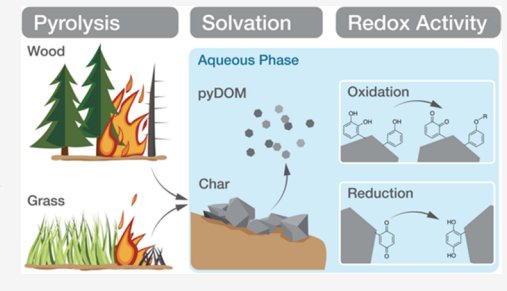
ACCESS

Metrics & More



Supporting Information

ABSTRACT: Chars are ubiquitous in the environment and release significant amounts of redox-active pyrogenic dissolved organic matter (pyDOM). Yet, the redox properties of pyDOM remain poorly characterized. This work provides a systematic assessment of the quantity and redox properties of pyDOM released at circumneutral pH from a total of 14 chars pyrolyzed from wood and grass feedstocks from 200 to 700 °C. The amount of released pyDOM decreased with increasing pyrolysis temperature of chars, reflecting the increasing degree of condensation and decreasing char polarity. Using flow-injection analysis coupled to electrochemical detection, we demonstrated that electron-donating capacities (EDC_{pyDOM}; up to 6.5 mmol_e—g_C⁻¹) were higher than electron-accepting



(EDC_{pyDOM}; up to 6.5 mmol_e-·g_C⁻¹) were higher than electron-accepting capacities (EAC_{pyDOM}; up to 1.2 mmol_e-·g_C⁻¹) for all pyDOM specimens. The optical properties and low metal contents of the pyDOM implicate phenols and quinones as the major redox-active moieties. Oxidation of a selected pyDOM by the oxidative enzyme laccase resulted in a 1.57 mmol_e-·g_C⁻¹ decrease in EDC_{pyDOM} and a 0.25 mmol_e-·g_C⁻¹ increase in EAC_{pyDOM}, demonstrating a largely irreversible oxidation of presumably phenolic moieties. Non-mediated electrochemical reduction of the same pyDOM resulted in a 0.17 mmol_e-·g_C⁻¹ increase in EDC_{pyDOM} and a 0.24 mmol_e-·g_C⁻¹ decrease in EAC_{pyDOM}, consistent with the largely reversible reduction of quinone moieties. Our results imply that pyDOM is an important dissolved redox-active phase in the environment and requires consideration in assessing and modeling biogeochemical redox processes and pollutant redox transformations, particularly in char-rich environments.

KEYWORDS: electron-accepting and -donating capacities, electron transfer, flow-injection analysis, electrochemistry, phenols, quinones

■ INTRODUCTION

Thermally altered plant biomass (char) is ubiquitous in the environment and has long been recognized as an important geosorbent for organic compounds and inorganic species, including pollutants. 1-5 More recent work has revealed that chars are also redox-active by accepting and donating electrons and, thereby, participate in biogeochemical electron transfer processes and pollutant redox transformations.⁶⁻³¹ Chars accept electrons from anaerobic microbial respiration or from inorganic reductants in the environment (e.g., hydrogen sulfide). 10,11,13,14,19-22,24,29,30,32 Following reduction, chars may then transfer electrons to both organic and inorganic pollutants, thereby facilitating their reductive transformation. ^{10,11,20-22,24,29,30,32} Chars are also involved in electron transfer between microbial cells ^{8,16} or from metal-reducing bacteria to hematite or ferrihydrite. ^{13,19} In addition, electron transfer to and from chars was shown to mitigate emissions of the radiatively active trace gas N₂O from agricultural soils.^{7,28} The important role of chars in redox reactions has led to considerable interest in characterizing the redox chemistry and reactivity of chars. However, chars also release dissolved organic carbon (DOC), which herein we refer to as pyrogenic dissolved organic matter (pyDOM) (operationally defined as DOC from bulk chars that passes through 0.45 μ m

filters). $^{33-35}$ The released amounts of pyDOM are considered significant in the global carbon cycle: for instance, pyDOM is estimated to contribute $\sim 10\%$ of the riverine flux of DOC to the oceans. 36,37 Yet, compared to bulk chars and non-pyrogenic DOM, only a few studies have characterized the redox properties of pyDOM and have attempted to link these characteristics to the physicochemical properties of the corresponding chars from which the pyDOM originated.

Two recent studies quantified the electron-donating and -accepting capacities of various pyDOM specimens (EDC $_{\rm pyDOM}$ and EAC $_{\rm pyDOM}$) using a mediated electrochemical approach, thereby demonstrating that pyDOM, alike chars, are redox-active. ^{33,34} We herein define EDC $_{\rm pyDOM}$ and EAC $_{\rm pyDOM}$ as method-dependent (i.e., operationally defined) and carbon-normalized number of electrons that pyDOM donate to a specific oxidant or accept from a specific reductant, respectively. One of the two studies reported that pyDOM

Received: April 13, 2021 Revised: July 3, 2021 Accepted: July 6, 2021 Published: July 28, 2021





specimens from straw-derived chars formed at 400 °C showed much higher EDC $_{\rm pyDOM}$ (from 2.42 to 7.10 mmol $_{\rm e^-}\cdot \rm g_{\rm C}^{-1}$) than EAC $_{\rm pyDOM}$ (from 0.40 to 0.81 mmol $_{\rm e^-}\cdot \rm g_{\rm C}^{-1}$). The second study, however, reported much smaller EDC $_{\rm pyDOM}$ than EAC $_{\rm pyDOM}$ for pyDOM derived from wheat-straw biochar formed over pyrolysis temperatures of 300–700 °C. 33 Both EDC $_{\rm pyDOM}$ and EAC $_{\rm pyDOM}$ exhibited maxima in this temperature series at 500 °C with values of 0.14 and 0.31 mmol $_{\rm e^-}\cdot \rm g_{\rm C}^{-1}$, respectively. 33

However, several central aspects of pyDOM redox properties remain unaddressed by previous work. To date, a systematic appraisal of the relationship between char provenance, pyrolysis temperatures, and redox capacities of pyDOM remains missing. Such characterizations are essential to link the quantity and redox properties of pyDOM to the physicochemical properties of the respective chars. This aspect is critical to better understand and predict the role of pyDOM in electron transfer reactions in char-rich systems. Second, a comparative analysis of the redox properties of a diverse set of pyDOM to the redox properties of the corresponding chars has not yet been conducted. Comparing the EAC and EDC values of pyDOM to those of chars will inform whether pyDOM may act as a significant redox buffer or whether its primary role is as an electron transfer mediator between other redox-active geochemical phases and species. Third, past work focused on quantifying the EDC and EAC values of a given pyDOM specimen, whereas studies following changes in pyDOM redox states during oxidation and reduction reactions involving pyDOM are missing. Such studies are important because they provide critical information on the reversibility of electron transfer to and from pyDOM.

Accordingly, the goal of this work was to provide a systematic assessment of pyDOM quantity, redox property, and reactivity, addressing the above-listed critical aspects. More specifically, we aimed at (1) understanding how feedstock materials and pyrolysis temperature of chars affect the amounts and redox properties of char-derived pyDOM, (2) comparing the redox capacities of pyDOM to those of the corresponding chars, and (3) elucidating changes in the redox states of pyDOM and assessing electron transfer reversibility to and from the pyDOM when undergoing oxidation and reduction reactions. We addressed the first two aims by quantifying the amounts of pyDOM and characterizing the optical and redox properties of pyDOM released from a total of 14 suspended chars that were prepared from grass or wood feedstocks over pyrolysis temperatures from 200 to 700 °C. Compared to the previous two studies on pyDOM redox properties, the set of pyDOM studied herein is considerably larger and more diverse in terms of both feedstock materials and range of char pyrolysis temperatures (i.e., 200-700 °C). Furthermore, we extracted the 14 pyDOM from chars of which we previously characterized the physicochemical properties³⁸ and redox characteristics. 15 This experimental design allowed us to compare the EAC and EDC of the pyDOM to those of the original source chars, a comparison that was missing from previous studies. To accomplish the third aim, we followed changes in EDC and EAC of a selected pyDOM during its enzymatic oxidation and non-mediated electrochemical reduction. All EAC and EDC analyses of pyDOM were conducted using a novel flow-injection analysis (FIA) system coupled to electrochemical detection.^{39,40} The exceptionally high sensitivity of this analytical approach allowed us to analyze pyDOM directly without the need to concentrate pyDOM prior to

redox analysis, as required in past studies which used mediated electrochemical reduction and oxidation (MER and MEO). 33,34

MATERIALS AND METHODS

Chemicals. Detailed information for all chemicals used is provided in Text S1.

Extracting pyDOM from Chars. We obtained pyDOM from a total of 14 different chars. Twelve of the 14 chars were from two series of six chars, each prepared from either grass (Festuca arundinacea) or wood (Pinus ponderosa) feedstock over a range of pyrolysis temperatures (i.e., charring for 1 h under oxygen-limited conditions at 200, 300, 400, 500, 600, or 700 °C).³⁸ The chars are herein abbreviated as WX and GX, where W and G refer to wood and grass feedstock, and X corresponds to the pyrolysis temperature. We additionally extracted pyDOM from two reference chars from rice (Oryza sativa Arborio) straw and chestnut (Castanea sativa) wood produced by pyrolysis under an N₂-atmosphere at 450 °C for 5 h (abbreviated as RS450 and CW450, respectively).⁴¹ The physicochemical properties of all chars, including their redox properties, have been extensively characterized in previous studies. 15,38 Key properties, including elemental composition, H/C and O/C ratios, and double-bond equivalence (DBE) are provided in Table S1.

To obtain pyDOM, we suspended chars at 15 g·L⁻¹ in a pH 7 buffered solution (10 mM phosphate) in batch reactors, followed by agitating the suspensions at 25 °C for 24 h in the dark on an end-to-end rotator (Heidolph Reax, Germany) at 100 rpm. We chose to extract pyDOM in pH 7 buffered solutions because pH 7 is environmentally relevant and because pH is expected to affect both the amount and chemical composition of DOM extracted from chars. 42,43 The samples were subsequently centrifuged at 4500 rpm for 10 min (Eppendorf 5804R, Germany) to remove chars from the aqueous phase. We collected the supernatant and passed it through syringe filters (polypropylene, 0.45 µm, Pall, Switzerland; all pre-rinsed with deionized water) to obtain the final pyDOM solutions. We confirmed stable solution pH over the course of the extraction (i.e., pH 7.0 ± 0.1 of the final solutions). The filtered pyDOM solutions were used in all subsequent experiments without any additional treatment except for solution pH adjustments for specific experiments. We acknowledge that the obtained pyDOM may contain structurally diverse components, such as organic (macro-)molecules that dissolved either from the bulk char or from condensates on the char that formed during the pyrolysis process. In addition, pyDOM as defined herein may contain char nanoparticles that detached from the bulk chars and passed through the 0.45 μ m cutoff filters. Such nanoparticles may have been released preferentially from high-temperature chars given that such chars contain abundant microcrystallite structures.^{38,44} We herein did not direct efforts toward identifying whether pyDOM contained these different components nor toward separately assessing their redox properties. Such detailed studies were beyond the scope of this work and would have required substantially more pyDOM (and hence bulk char material) than was available to us. Instead, we report and discuss EAC and EDC values of the pyDOM in its entirety as it was obtained but highlight interpretational challenges that result from the heterogeneity of pyDOM.

Properties of pyDOM. We collected UV-visible lightabsorption spectra of the filtered pyDOM solutions from 190 to 800 nm on a Varian Cary 100 Bio (Agilent). We further determined the nonpurgeable organic carbon (NPOC) concentrations of the pyDOM solutions using a total organic carbon analyzer (TOC-L, Shimadzu). The specific ultraviolet absorbance (SUVA₂₅₄, L·mg⁻¹·m⁻¹) of each pyDOM was calculated by dividing its ultraviolet absorbance at 254 nm $(A_{254}, \text{ cm}^{-1})$ by its NPOC $(\text{mg}\cdot\text{L}^{-1})$. Finally, we determined the total Fe and Mn concentrations in the pyDOM specimens using inductively coupled plasma optical emission spectrometry (ICP-OES, Vista MPX, Varian, Australia).

Redox Characterization of pyDOM. The EDC_{pvDOM} and EAC_{pvDOM} values were determined on a recently introduced FIA system coupled to electrochemical flow-through detectors, as previously described. ^{39,40} Briefly, the FIA system contained an oxidative and a reductive solution flow path operated in parallel for EDC and EAC determination, respectively. Each flow path consisted of a reagent stream (containing either the oxidant diammonium 2,2'-azino-bis(3-ethyl-6-benzothiazolinesufonate) radical (ABTS^{•+}) or the reductant N,N'-bis(3sulfonatopropyl)-4,4'-bipyridinium radical (ZiV*-) and a carrier stream (0.1 M phosphate buffer and 0.1 M KCl at pH 7)). We used ABTS^{•+} and ZiV^{•-} as the oxidant and reductant of electron-donating and -accepting moieties in the pyDOM, respectively, because these chemicals have high and low standard reduction potentials ($E_{\rm H}{}^0=+0.70~{\rm V}$ for the ABTS $^{\bullet+}/{\rm ABTS}$ and $E_{\rm H}{}^0=-0.41{\rm V}$ for ZiV/ZiV $^{\bullet-}$ redox couples) and were previously shown to undergo fast oneelectron transfer with redox-active moieties in DOM. 39,40 Reduction potentials (E) were measured against Ag/AgCl reference electrodes but were reported herein relative to the standard hydrogen electrode $(E_{\rm H})$. All electrochemical measurements were conducted using two potentiostats (models 630C and 630D, CH Instruments, Austin, TX).

All FIA measurements were performed in an anoxic glovebox (N_2 atmosphere, $p_{O_2} < 1$ ppm). We first adjusted both the pH and the ionic composition of pyDOM samples to match that of the carrier stream in the FIA system prior to the analysis. We then loaded each sample into two injection loops of identical volumes (100 μ L) on a 10-port/2-position injector valve (Qmix V, Cetoni, Germany). The carrier streams were diverted through the injection loops to deliver the sample into the two flow paths of the FIA system. The carrier streams were subsequently mixed with the reagent streams containing ABTS* or ZiV*. The mixed solutions were passed through 10-m Teflon knitted reaction coils (Biotech, Sweden) to result in a reaction time of 25 min between the pyDOM and the oxidant or reductant. Reduction of ABTS of and oxidation of ZiV by electron transfer from electron-donating and to electron-accepting moieties in pyDOM resulted in the formation of ABTS and ZiV. Following the reaction coils, each stream passed through an electrochemical flow-cell containing glassy carbon working electrodes (ALS, Japan) operated in chronoamperometry mode with constant applied $E_{\rm H}$ (i.e., $E_{\rm H}$ = +0.71 and -0.43 V for the oxidative and reductive streams, respectively). In the electrochemical detectors, the ABTS and ZiV formed by reaction with pyDOM, resulting in oxidative and reductive current peak responses, respectively. We integrated these current peak responses over time and converted peak areas to the number of electrons transferred from and to pyDOM (i.e., EDC_{pyDOM} and

 EAC_{pvDOM} ($\mu mol_{e-} \cdot L^{-1}$)) by calibrating the current peak responses using the EDC and EAC standards ascorbate and 9,10-anthraquinone-2,6-disulfonate (2,6-AQDS) (i.e., ED-7,10-anthraquinone-2,0-disultonate (2,6-AQDS) (i.e., ED- $C_{ascorbate} = 2.00 \text{ mol}_{e-} \cdot \text{mol}_{ascorbate}^{-1}$ and EAC_{AQDS} = 2.00 mol_{e-} \text{mol}_{AQDS}^{-1}) (Figure S4). We also compared the obtained EDC_{pyDOM} and EAC_{pyDOM} to the respective EDC_{char} and EAC_{char} values (mmol_{e-} \(\text{g}_{char}^{-1} \)) of the bulk chars previously determined unique moletics. determined using mediated electrochemical reduction (MER) and oxidation (MEO)¹⁵ under comparable redox conditions (pH 7 and $E_{\rm H}$ of +0.61 and -0.49 V using ABTS and ZiV as electron transfer mediators in MEO and MER, respectively).

Redox Transformations of pyDOM. For the pyDOM obtained from the grass char formed at 400 °C (i.e., G400), we followed changes in its redox states while it underwent two types of redox reactions, namely, its oxidation by phenol oxidase laccase and its non-mediated electrochemical reduction in a bulk electrochemical reduction cell. We chose the pyDOM from G400 because it had comparatively high EDC_{pyDOM} and EAC_{pvDOM} values and low redox-active metal contents (see below).

Enzymatic Oxidation of pyDOM. We incubated the pyDOM solution with laccase from Trametes versicolor (activity 22.4 U/mg, product number 53793 from Fluka), which catalyzes the oxidation of phenolic and hydroquinone moieties in the presence of oxygen as the co-substrate. 46 Experiments were run in duplicates. We first lowered the pH of the pyDOM solution from pH 7.0 to 4.6 (using a 100 mM acetate buffer at pH 4.6), at which the laccase had high activity. 46 We then added laccase from a freshly prepared stock solution. The calculated initial activity of laccase in the batch reactors was 0.99 U/mL, based on the information provided by the vendor, and the ratio of enzyme activity to NPOC was 9.69 U/mg_C . All samples were subsequently incubated on a horizontal shaker (Kühner, Switzerland) at 300 rpm and 25 °C for 2 days. Laccase-free controls containing only pyDOM were set up at the same time and handled identically. Over the course of the incubation period, we repeatedly withdrew 800-µL aliquots and immediately purged them with N2 to remove O2 and thereby quench laccase activity. For quantifying changes in the redox state of the pyDOM_{G400} in the aliquots on the FIA system, we subsequently adjusted their pH and ionic composition to that of the carrier solution in the FIA system using a concentrated phosphate buffer solution (200 mM, pH 7) prior to the analysis.

Non-mediated Electrochemical Reduction of pyDOM. We also followed changes in the redox state of $pyDOM_{G400}$ during non-mediated electrochemical reduction.³⁹ These reductions were carried out in an anoxic glovebox (N_2 atmosphere, p_{O_2} < 1 ppm). We first diluted pyDOM_{G400} to a concentration of 43.2 $g_C \cdot L^{-1}$ in a pH 7 buffer (10 mM phosphate) and transferred 10 mL of the solution into a 25 mL glassy carbon working electrode (WE) cylinder (Sigradur G, HTW, Germany) with an Ag/AgCl reference electrode (ALS, Japan). A platinum wire served as the counter electrode and was separated from the WE compartment by a porous glass frit. The electrochemical reduction of $pyDOM_{G400}$ was carried out at an applied reduction potential of $E_{\rm H}$ = -0.47 V while continuously monitoring the reductive current. The reduction was terminated after 24 h when the reductive current had returned to a background current value of around 1.5×10^{-8} A, which was independently determined for pyDOM_{G400}-free solutions with otherwise the same composition and pH. At

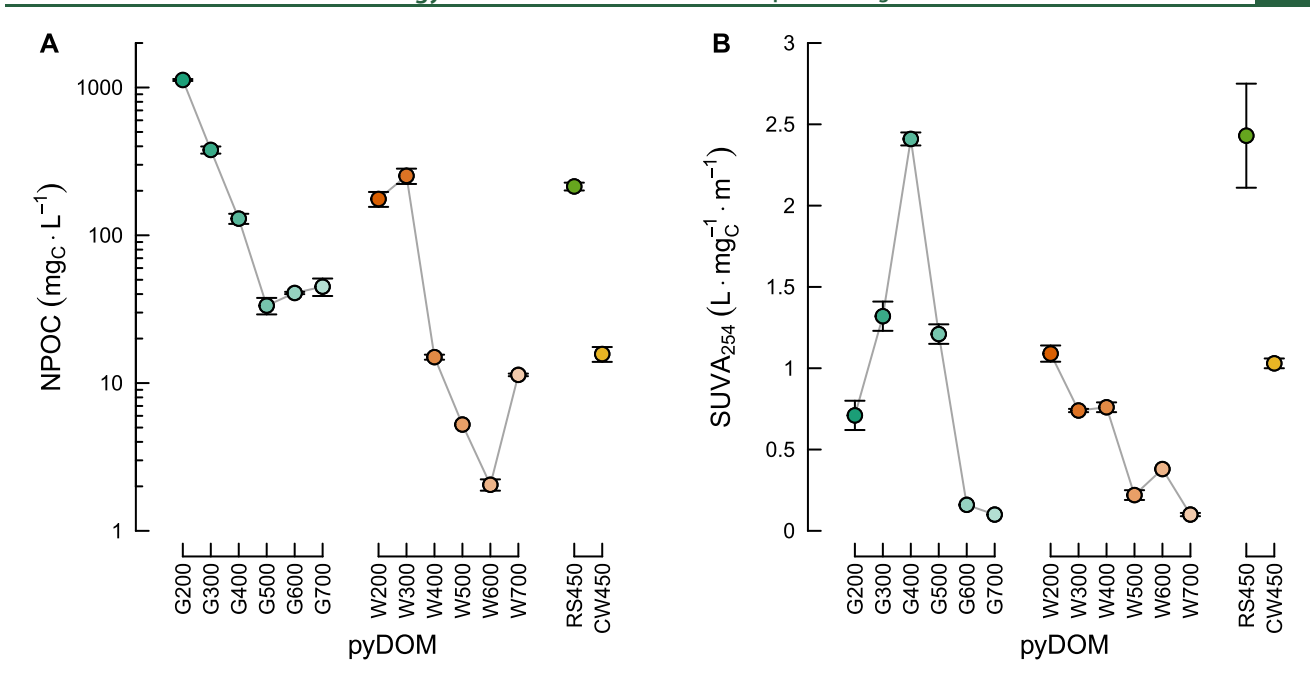


Figure 1. (A) Nonpurgeable organic carbon (NPOC, $mg_C \cdot L^{-1}$) concentrations and (B) the specific ultraviolet absorbance (SUVA₂₅₄, L· $mg_C^{-1} \cdot m^{-1}$) of pyDOM obtained from two temperature-series chars prepared from grass (G) and wood (W) feedstock as well as from two reference char materials RS450 and CW450. GX and WX represent temperature-series grass and wood chars prepared at different pyrolysis temperatures X (in °C), respectively. The reference chars were prepared by pyrolyzing rice straw (*Oryza sativa* Arborio) and chestnut wood (*Castanea sativa*) at 450 °C. Error bars represent the standard deviation from experimental duplicates.

different time intervals during the electrochemical reduction of the pyDOM $_{\rm G400}$ solutions, we withdrew 800- μ L aliquots from the cell. The pH and ionic composition of these aliquots were adjusted following the protocol described above. We subsequently analyzed the pyDOM $_{\rm G400}$ solution aliquots on the FIA system.

■ RESULTS AND DISCUSSION

NPOC and SUVA₂₅₄ Values of pyDOM from Chars. Figure 1 shows the NPOC (panel A) and SUVA₂₅₄ (panel B) values for all pyDOM specimens. The NPOC range of pyDOM spanned ~1.5 and 2 orders of magnitude from the highest to lowest values for the G and W series, respectively (note the logarithmic ordinate scale in Figure 1A). As alluded to above, the NPOC is herein considered a sum parameter for pyDOM, acknowledging that the pyDOM may contain structurally diverse components, including char nanoparticles. Based on NPOC values, the grass chars released more pyDOM than the wood chars at any given pyrolysis temperature. The NPOC values of pyDOM released from both wood and grass chars decreased with increasing pyrolysis temperature (with the exception of an increase in NPOC from W600 to W700 pyDOM, as detailed below). For both series, the most pronounced decrease in NPOC values occurred between chars formed at low (200-300 °C) and intermediate (500 °C) temperatures. For the two additional reference chars, the pyDOM released from the grass char RS450 also showed a higher NPOC value than the one from the wood char CW450. We estimated the percentage of the respective char carbon dissolved as pyDOM by the ratio of the pyDOM NPOC over the amount of carbon in the bulk char at the specific suspension concentration (details of the calculation are provided in Text S2) and plotted the data in Figure S1. The fraction of char carbon dissolved as pyDOM decreased with increasing pyrolysis temperature, with an estimated 15.9%

from the low-temperature char and 0.3% from the high-temperature char, consistent with the trends reported in previous studies. 42,43

For the grass char series, the SUVA254 values of pyDOM samples increased with increasing pyrolysis temperature from G200 to G400 and subsequently decreased from G400 to G700. By comparison, the SUVA₂₅₄ values of pyDOM obtained from wood chars continuously decreased with increasing pyrolysis temperature from W200 to W700. We note that past work reported positive correlations between SUVA₂₅₄ values and aromaticity, as determined by ¹³C NMR, for DOM isolates from aquatic and terrestrial environments.⁴⁷ Assuming that this correlation also applies to pyDOM (which likely is the case for pyDOM dominated by truly dissolved organic (macro-)molecules but may not hold true for char nanoparticles), the aromaticity was estimated to range from 4 to 19% for pyDOM from both grass and wood chars (details provided in Text S3). We also calculated the absorbance ratios at 250 nm over 365 nm (i.e., $E_2 \cdot E_3^{-1}$) for all pyDOM specimens. We chose $E_2 \cdot E_3^{-1}$ because this ratio was previously shown to decrease with increasing DOM molecular size (i.e., DOM absorption shifts to higher wavelengths with increasing DOM molecular weight). 48 In lieu of direct determinations of pyDOM molecular weight (e.g., by size exclusion chromatography or sequential centrifugal filtration of pyDOM solutions), we expect that the $E_2 \cdot E_3^{-1}$ is also indicative of the molecular weight of "dissolved" pyDOM (but unlikely for char nanoparticles, if present in pyDOM from high-temperature chars). As shown in Figure S2, the $E_2 \cdot E_3^{-1}$ ratios of pyDOM obtained from grass chars increased from G200 to G700, suggesting that the average molecular weight of pyDOM decreased with increasing pyrolysis temperature. By comparison, no apparent trend was observed for $E_2 \cdot E_3^{-1}$ of pyDOM from wood chars with respect to pyrolysis temperatures.

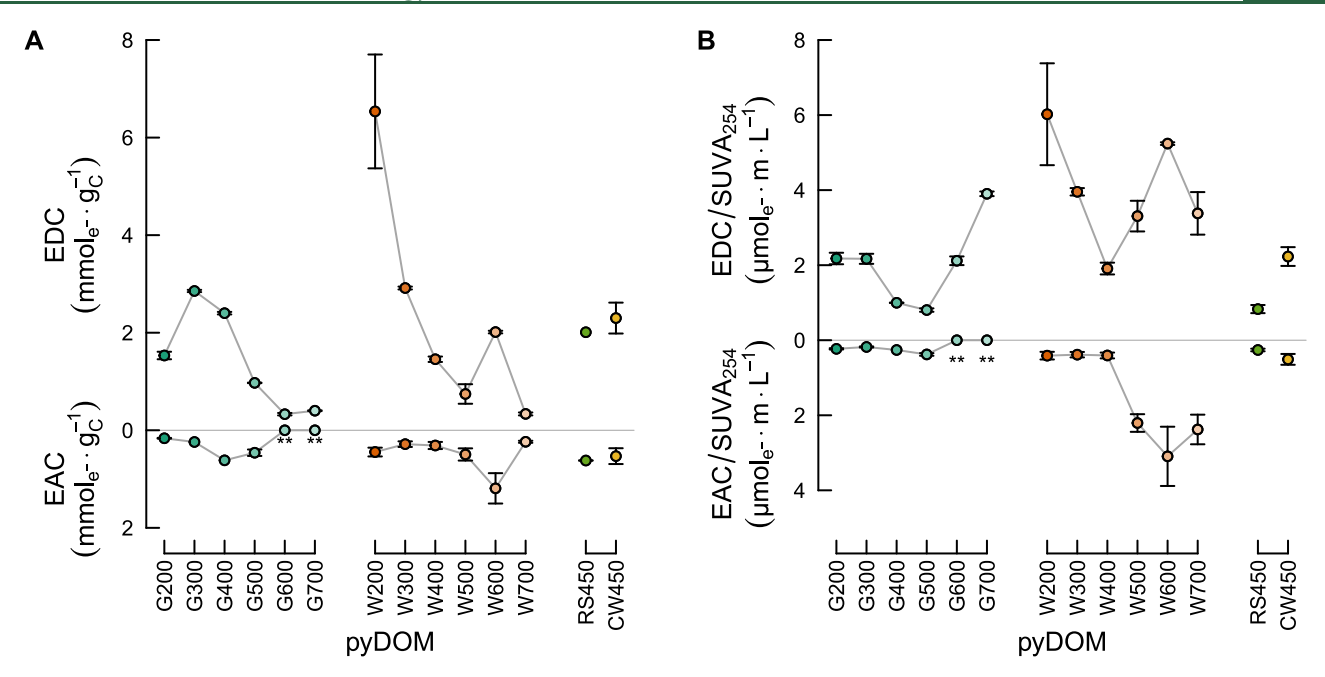


Figure 2. (A) Nonpurgeable organic carbon (NPOC)-normalized EDC and EAC (mmol_e- \cdot g_c⁻¹) and (B) specific ultraviolet absorbance-normalized EDC and EAC values (μ mol_e- \cdot m·L⁻¹) of pyDOM obtained from 14 chars as a function of the pyrolysis temperature of chars and source materials. ** indicates that the obtained values were below the limits of quantification. Error bars represent the standard deviation from experimental duplicates.

We rationalize the above trends in NPOC and SUVA₂₅₄ values of pyDOM specimens with pyrolysis temperature on the basis of differences in the physicochemical properties of the corresponding bulk chars. Compared to wood, grass generally has higher contents of polar and non-aromatic cellulose and hemicellulose components and lower content of aromatic lignin components. 49,50 Therefore, the comparatively higher NPOC and lower SUVA₂₅₄ values of pyDOM from the lowtemperature grass than wood char (G200 vs. W200) likely reflected the higher polarity and lower aromaticity of the grass feedstock. We note that differences in the NPOC and SUVA254 values of grass- and wood-derived pyDOM may also reflect differences in the responses of these materials to temperature: while pyrolysis of hemicellulose and cellulose was reported to primarily occur between 200 and 400 °C, pyrolysis of lignin seems to occur over a wider temperature range (from 160 to 900 °C). 51 As pyrolysis temperature increased from 200 to 400 °C, the polarity of grass chars decreased while aromaticity increased, as evidenced by decreasing H/C and O/C ratios and increasing double-bond equivalents (DBE) of the chars (Table S1³⁸). This decrease in polarity and increase in aromaticity likely lowered the fraction of the char that was water-soluble as pyDOM but increased pyDOM aromaticity, consistent with the measured decreases in NPOC values and the increases in SUVA₂₅₄ values for pyDOM obtained from grass chars (G200 to G400). The highest pyrolysis temperatures of 600 and 700 °C led to polycondensation reactions in the grass chars and further decreased their oxygen contents (G600 and G700).³⁸ The decrease in SUVA₂₅₄ values of pyDOM from G400 to G700 is inversely correlated to the increases in DBE of these chars (Figure S3). These findings suggest that the pyDOM, released in low amounts from high-temperature chars, was primarily of aliphatic character. Alternatively, it is possible that the pyDOM from G600 and G700 contained char nanoparticles. The latter could have contributed to the slight increase in NPOC from G400 to G700 pyDOM (we note that

lower molar absorbance values of aromatic groups in char nanoparticles would explain the decrease in $SUVA_{254}$ values despite the fact that char nanoparticles from high-temperature chars are expected to have a high aromatic carbon content).

Similarly, we ascribe the general decrease in the NPOC values of pyDOM from W200 to W600 to the decreases in oxygen contents and increases in aromaticity of the bulk wood chars (Table S1³⁸). The increase in NPOC of pyDOM from W600 to W700 may indicate increased release of char nanoparticles from highly condensed, graphitic W700. SUVA₂₅₄ values of pyDOM from wood chars also decreased as the DBE of bulk materials increased from W200 to W600 (Figure S3). These findings suggest that the pyDOM released in low amounts from high-temperature chars either contained low aromaticity or that it had a higher contribution of char nanoparticles with comparatively low molar absorbance coefficient at 254 nm (and hence low SUVA₂₅₄ values).

Redox Properties of pyDOM. Figure 2A shows the EDC_{pyDOM} and EAC_{pyDOM} values that were normalized to their NPOC values. This normalization allows for the comparison of redox properties of different pyDOM on the basis of their carbon concentrations. All pyDOM had quantifiable EDC values and thus contained DOM moieties or inorganic species that donated electrons to the chemical oxidant ABTS*+. All pyDOM specimens, except those released from G600 and G700, accepted electrons from the chemical reductant ZiV*and thus contained reducible organic moieties or inorganic species. While the pyDOM from G600 and G700 also showed reductive current responses in the FIA system, these responses were too small to be accurately quantified. This finding suggests that these pyDOM specimens contained only low concentrations of char nanoparticles because the latter would be expected to accept electrons given the EAC values of the bulk chars from which these particles originate. 15 We summed the EDC_{pyDOM} and EAC_{pyDOM} values to determine the

Table 1. Total Concentrations of Iron (Fe) and Manganese (Mn) in pyDOM Obtained from 14 Char Specimens and the Estimated Contribution from Metals to the Overall Electron-Exchange Capacity (EEC) of pyDOM (%)

	metal content $(\mu g/L)^a$		$EEC_{Mn} (\mu mol_{e}^{-}/L)^{b}$		$EEC_{Fe} (\mu mol_{e^{-}}/L)^{b}$		metal contribution to EEC_{pyDOM} (%)		
samples	Mn	Fe	Mn^{2+}/Mn^{3+}	Mn^{2+}/Mn^{4+}	Fe ²⁺ /Fe ³⁺	$EEC_{pyDOM} (\mu mol_{e}^{-}/L)^{c}$	Mn^{2+}/Mn^{3+}	Mn^{2+}/Mn^{4+}	$\mathrm{Fe^{2+}/Fe^{3+}}$
G-700	0.07	0.07	0.00	0.00	0.00	17.99	0.01	0.01	0.01
G-600	0.01	NA	0.00	0.00	NA	13.44	0.00	0.00	NA
G-500	0.01	NA	0.00	0.00	NA	47.73	0.00	0.00	NA
G-400	0.01	NA	0.00	0.00	NA	390.88	0.00	0.00	NA
G-300	0.86	1.47	0.02	0.03	0.03	1170.39	0.00	0.00	0.00
G-200	10.60	15.30	0.19	0.39	0.27	1907.54	0.01	0.02	0.01
W-700	93.87	9.87	1.71	3.41	0.18	6.49	26.29	52.58	2.72
W-600	119.58	10.52	2.17	4.35	0.19	6.61	32.89	65.78	2.84
W-500	34.79	12.09	0.63	1.27	0.22	6.50	9.74	19.47	3.32
W-400	23.99	14.41	0.44	0.87	0.26	26.48	1.65	3.29	0.97
W-300	45.10	17.38	0.82	1.64	0.31	808.23	0.10	0.20	0.04
W-200	65.59	19.86	1.19	2.39	0.35	1216.06	0.10	0.20	0.03
RR450	102.41	40.13	1.86	3.72	0.72	562.23	0.33	0.66	0.13
CW450	3.42	19.85	0.06	0.12	0.35	43.99	0.14	0.28	0.81

^aConcentrations were obtained from ICP-OES measurements; the limits of quantification (LoQ) for Mn and Fe were 0.02 and 0.1 μ g·L⁻¹, respectively. ^bEEC values originated from Fe (EEC_{Fe}) were calculated by assuming an exchange of 1 mol e⁻ per mole Fe (i.e., redox couple Fe³⁺/ Fe²⁺), while EEC values originated from Mn (EEC_{Mn}) were calculated by assuming and the exchange of either 2 or 1 mol e⁻ per mole Mn (i.e., for redox couples Mn⁴⁺/Mn²⁺, Mn⁴⁺/Mn³⁺, or Mn³⁺/Mn²⁺). ^cEEC_{pyDOM} (μ mol_e·L⁻¹) = EDC_{pyDOM} + EAC_{pyDOM}, which were measured using an FIA system coupled to electrochemical detection.

electron-exchange capacity (EEC) of the pyDOM samples (Table 1).

To assess contributions from redox-active inorganic species to the measured EDC_{pyDOM} and EAC_{pyDOM} , we quantified concentrations of iron (Fe) and manganese (Mn) (Table 1), which were presumably the two major redox-active elements present.⁵² Total Mn and Fe concentrations were low in all pyDOM from the grass chars. By comparison, Mn and Fe concentrations were higher in pyDOM from all wood chars and reference chars (RS450 and CW450). For quantitative considerations, we assumed an exchange of 1 mol_e per mol_{Fe} (i.e., redox couple Fe³⁺/Fe²⁺) and either 2 or 1 mol_e per mol_{Mn} (i.e., redox couples Mn⁴⁺/Mn²⁺, Mn⁴⁺/Mn³⁺, or Mn³⁺/ Mn²⁺). Table 1 shows that the contribution of Fe to EEC_{pyDOM} was negligible for all pyDOM (<5%). Likewise, Mn had insignificant contributions to the EEC_{pyDOM} obtained from all grass chars, low-temperature wood chars (W200, W300, and W400), and both reference chars (<5%). For pyDOM obtained from high-temperature wood chars (W500, W600, and W700), we estimated that Mn may have had larger contributions to the $\text{EEC}_{\text{pyDOM}}$ ca. 10–20% for pyDOM from W500, 33-66% for pyDOM from W600, and 26-53% for pyDOM from W700. This finding implies that NPOCnormalized EDC_{pyDOM} and EAC_{pyDOM} values from hightemperature chars (W500 to W700) need to be carefully interpreted given their elevated Mn contents. However, even for these pyDOM specimens, the data supports that organic moieties largely contribute to the electron-accepting and -donating capacities, either in the form of truly dissolved organic (macro-)molecules and/or of char nanoparticles.

Figure 2A shows that pyDOM released from grass chars donated and accepted up to 2.86 and 0.62 $\rm mmol_{e^-}\cdot g_C^{-1}$, respectively. By comparison, the pyDOM from wood chars exhibited even higher EDC_{pyDOM} and EAC_{pyDOM}, donating and accepting up to 6.5 and 1.2 $\rm mmol_{e^-}\cdot g_C^{-1}$, respectively. Regardless of the source material and the pyrolysis temperature of the chars, the EDC_{pyDOM} of the corresponding pyDOM was

consistently higher than its EAC_{pvDOM}, suggesting that pyDOM contained more oxidizable (presumably phenolic) moieties than reducible (presumably quinone) moieties. These findings are consistent with a previous study reporting EDC values from 2.42 to 7.10 $\text{mmol}_{\text{e-}} \cdot g_{\text{C}}^{-1}$ for pyDOM from crop-derived chars formed at 400 °C, while their corresponding EAC were smaller and varied between 0.4 and 0.8 mmol_e- g_C^{-1,34} However, another study reported much smaller EDC (up to 0.14 $\text{mmol}_{\text{e-}} \cdot \text{g}_{\text{C}}^{-1}$) and EAC values (up to 0.31 $\text{mmol}_{\text{e-}} \cdot \text{g}_{\text{C}}^{-1}$) for pyDOM derived from wheat-straw biochar.³³ These differences may result from a range of factors, including feedstocks, pyrolysis conditions, extraction protocols, and the analytical method used to determine EAC and EDC values (e.g., pH, $E_{\rm H}$, and the choice of redox mediators). Our work largely extends on past studies on pyDOM redox properties in that we herein demonstrate the presence of electron-donating and -accepting organic moieties in a very large and diverse set of pyDOM specimens that we obtained from source chars formed from different feedstocks and over a broad range of pyrolysis temperatures. As such, we conclude that pyDOM are generally redox-active, akin to terrestrial and aquatic DOM.^{39,53}

For pyDOM obtained from grass chars, both EDC_{pyDOM} and EAC_{pyDOM} increased with increasing pyrolysis temperature of chars from 200 to 300–400 $^{\circ}$ C but, above these temperatures, decreased with increasing temperature. By comparison, EDC_{pyDOM} and, in a less pronounced manner, EAC_{pyDOM} of pyDOM from wood chars decreased from the largest values for W200 to much smaller values for W400 and W500. While EDC_{pyDOM} and EAC_{pyDOM} values for pyDOM from W500 to W600 increased, these increases possibly reflect the elevated concentrations of Mn in these samples (Table 1).

We postulate that the differences in the redox properties of pyDOM collected from low-temperature grass and wood chars primarily reflected the differences in chemical compositions of the feedstock, modulated by pyrolysis temperature: as discussed above, the higher EDC_{pyDOM} of pyDOM from

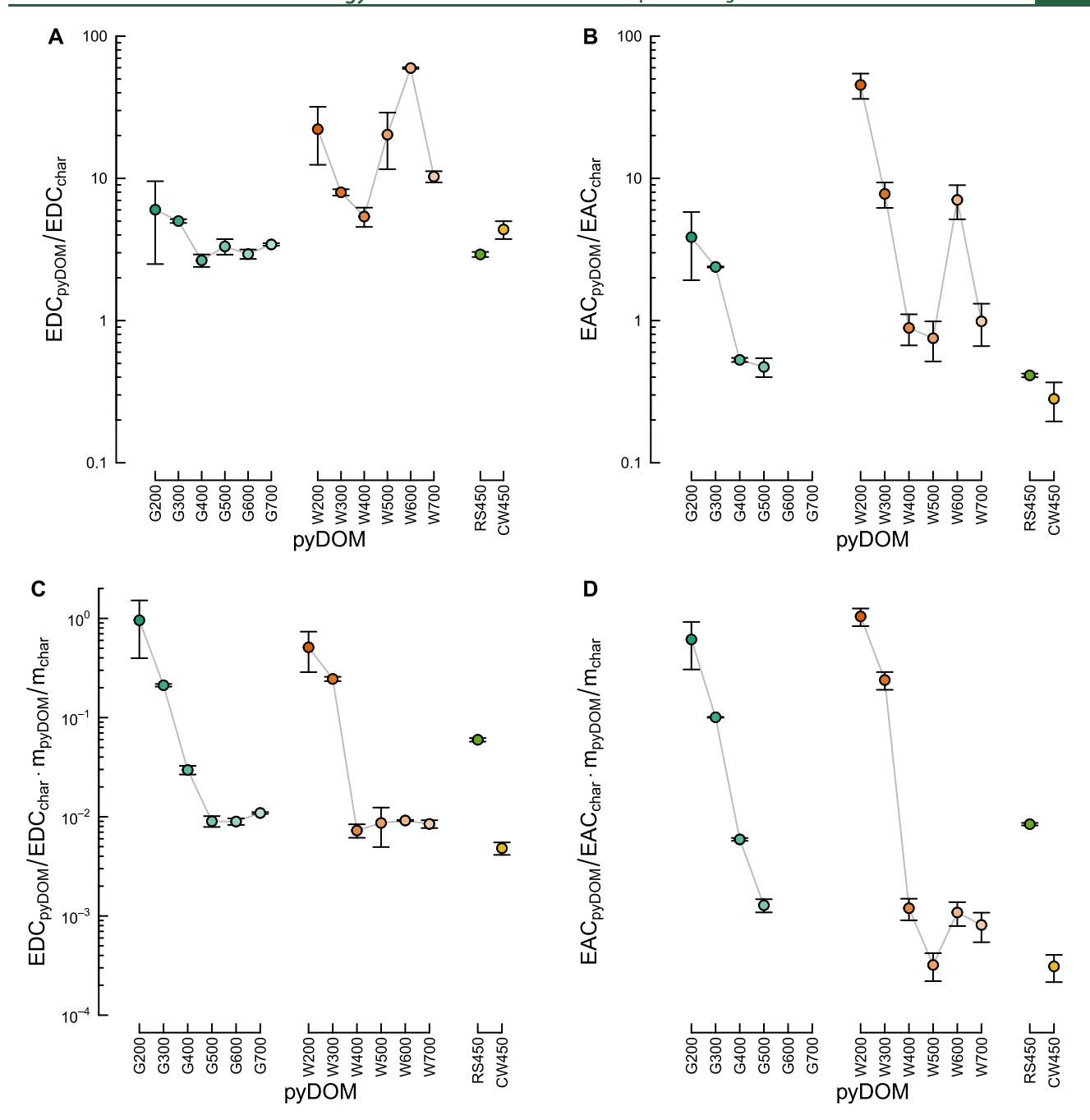


Figure 3. Ratios of the (A) EDC_{pyDOM}/EDC_{char} and (B) EAC_{pyDOM}/EAC_{char} based on mmole electrons exchanged per gram of carbon; ratios of (C) EDC_{pyDOM}/EDC_{char} and (D) EAC_{pyDOM}/EAC_{char} based on mmole electrons exchanged per gram of char with respect to source materials and pyrolysis temperatures. Detailed calculations are provided in Text S4. Note that the EDC_{pyDOM} and EAC_{pyDOM} shown here are the same as in Figure 2 but renormalized and plotted differently. The EDC_{char} and EAC_{char} of chars were previously quantified by Klüpfel et al. using the same electron transfer mediators (i.e., $EAEC_{char}$) under similar analysis conditions than used herein (i.e., EEC_{char}) EDC and EAC quantification at EEC_{char} and EEC_{char} bars represent the standard deviation from experimental duplicates.

W200 than G200 is consistent with the higher lignin contents in wood than grass and thus higher concentrations of electron-donating phenols in pyDOM from wood than those from grass. As the pyrolysis temperatures increased, thermally induced chemical changes in the chars, such as the decomposition of lignin phenols, could explain the overall decrease in the EDC_{pyDOM} values in both pyDOM sets with increasing pyrolysis temperature of the chars.

While all pyDOM samples were redox-active, there were considerable variations in EDC_{pyDOM} and EAC_{pyDOM} values among different pyDOM specimens (Figure 2A). These

variations are not unexpected, given that normalization to the total carbon content of the pyDOM does not adequately account for the fact that only a fraction of the total carbon is associated with redox-active moieties and that this fraction likely varies among pyDOM specimens. Given that phenol and quinone moieties are generally considered to dominate the redox capacity of DOM and given that the carbon in these moieties has aromatic character, we renormalized the EDC $_{\rm pyDOM}$ and EAC $_{\rm pyDOM}$ to their respective SUVA $_{254}$ values. As shown in Figure 2B, EDC $_{\rm pyDOM}/{\rm SUVA}_{254}$ and EAC $_{\rm pyDOM}/{\rm SUVA}_{254}$ values showed smaller overall variations among the

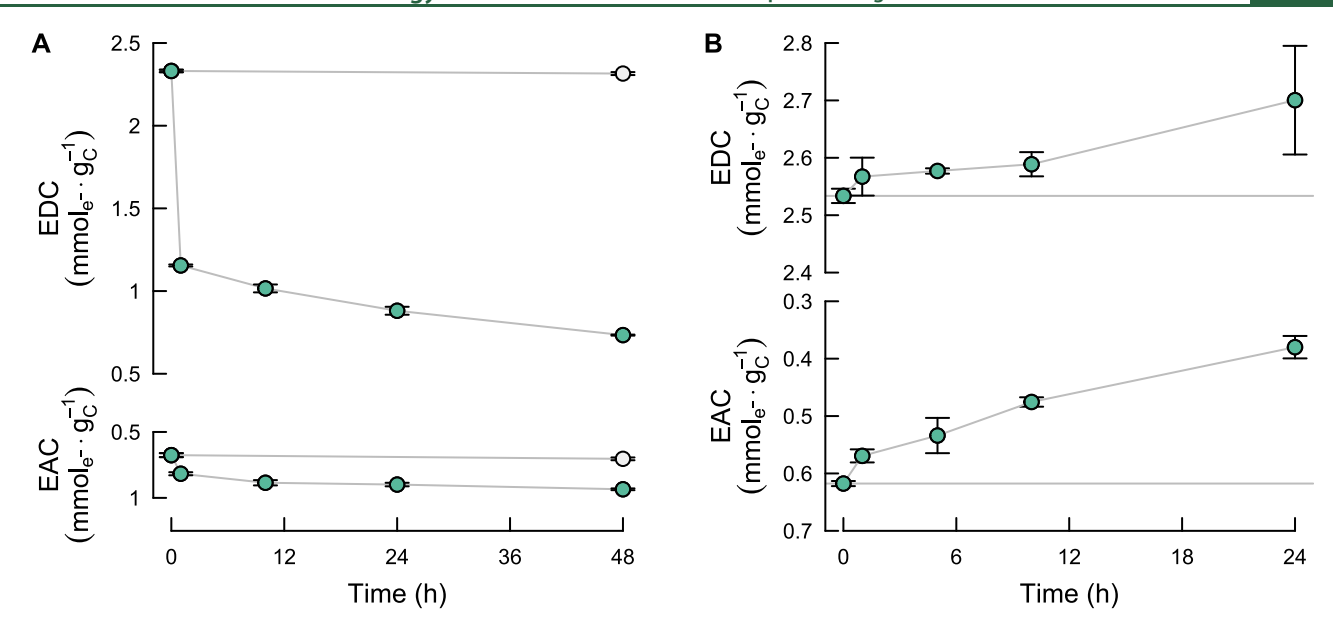


Figure 4. (A) Changes in the EDC and EAC values of pyDOM obtained from grass char G400 during the enzymatic oxidation at pH 4.6 with (filled circles) or without (circles) laccase from T. versicolor over 48 h. The activity of laccase in the batch reactors and the initial ratio of enzyme activity to the nonpurgeable organic carbon (NPOC) were 0.99 U/mL and 9.69 U/mg C, respectively. (B) Changes in the EDC and EAC values of pyDOM obtained from grass char G400 during the non-mediated electrochemical reduction ($E_{\rm H} = -0.59$ V, pH 7) over 24 h. The measured current of the reaction system returned to the background current of 1.5×10^{-8} A after 24 h. Error bars represent the standard deviation from experimental duplicates.

different pyDOM specimens. This is particularly evident for the pyDOM from the temperature series of wood chars: while the NPOC-normalized EDC_{pyDOM} varied by a factor of up to 20 (i.e., from 0.3 to 6.5 mmol_e- \cdot g_C⁻¹), the EDC_{pyDOM}/ SUVA₂₅₄ varied by only a factor of three (i.e., from 2 to 6 $mmol_{e^-}m\cdot L^{-1}$). The smaller variations of $EDC_{pyDOM}/SUVA_{254}$ and EAC_{pvDOM}/SUVA₂₅₄ support the assessment that the capacities of pyDOM to donate and accept electrons were linked to their contents of aromatic moieties. Thus, based on our findings and in line with results of previous studies on the redox properties of DOM in aquatic and terrestrial systems, 39,40,53 we propose that EDC_{pyDOM} and EAC_{pyDOM} are dominated by electron-donating phenolic and electronaccepting quinone moieties, respectively. At the same time, we acknowledge that the EDCpvDOM and EACpvDOM of pyDOM from high-temperature wood chars may have significant contributions from Mn. Furthermore, it is possible that char nanoparticles contributed to EDC_{pvDOM} and EAC_{pvDOM} values, particularly for the pyDOM derived from high-temperature chars. Future work is needed to assess the relative contributions of truly dissolved organic (macro-)molecules and of char nanoparticles to overall pyDOM and, if contributions change considerably with the pyrolysis temperature of the chars, to determine the redox properties of individual pyDOM components.

Comparison of the Redox Properties of pyDOM and Corresponding Chars. We obtained pyDOM from a set of chars for which we previously determined EAC_{char} and EDC_{char} values using the same electron transfer mediators and under similar analysis conditions used herein (i.e., pH 7; EDC and EAC quantification at $E_{\rm H} = +0.61$ and -0.49 V for chars and $E_{\rm H} = +0.71$ and -0.43 V for pyDOM). We, therefore, could compare trends in EAC and EDC values of pyDOM to their corresponding chars (Table S2). We first compared the EAC and EDC values of pyDOM with the chars based on mmole electrons exchanged per gram of carbon. Specifically, we

normalized the previously reported EDC_{char} and EAC_{char} values (mmol_e—' g_{char}^{-1}) of the chars¹⁵ to their carbon contents to obtain the same units as used herein for NPOC-normalized EDC_{pyDOM} and EAC_{pyDOM} of pyDOM (mmol_e—' g_{C}^{-1}) as described in Text S4. This comparison revealed much larger EDC_{pyDOM} and EAC_{pyDOM} than EDC_{char} and EAC_{char} (Figure 3A,B). Thus, pyDOM contained a larger number of redoxactive moieties on a per gram carbon basis than the chars from which pyDOM was obtained.

We also estimated the potential contributions of pyDOM to EDC_{char} and EAC_{char} if pyDOM was not extracted from the chars prior to their redox analyses. Notably, we used our experimental char mass to solution volume ratio (i.e., 15 g_{char}· L⁻¹) and the measured NPOC values of pyDOM. Details are provided in Text S4. Figure 3C,D shows that pyDOM may largely contribute to the EDC_{char} and EAC_{char} values of lowtemperature chars (200 and 300 °C) of both wood and grass. It is hence important to consider contributions from pyDOM to total redox capacities of chars, especially when analyzing low-temperature chars. As the pyrolysis temperature increased from 200 to 700 $^{\circ}\text{C}$, the ratios of both EDC $_{\text{pyDOM}}/\text{EDC}_{\text{char}}$ and EAC_{pyDOM}/EAC_{char} decreased and leveled off at low values (ratio of $\sim 0.01-0.001$). This comparison highlights that pyDOM made only small contributions to the redox capacities of bulk chars formed at higher temperatures. While this finding suggests that redox buffering by pyDOM in systems containing high-temperature chars may be small, the pyDOM may still act as a diffusive electron transfer shuttle that accelerates electron transfer to and from high-temperature chars.

Redox Transformation of Organic Moieties in pyDOM. We selected pyDOM collected from grass char G400 (pyDOM $_{\rm G400}$) as a model pyDOM for additional experiments that aimed at monitoring electron transfer from and to its redox-active moieties during biogeochemically relevant redox reactions. We chose pyDOM $_{\rm G400}$ because of its intermediate EDC $_{\rm pyDOM}$ and EAC $_{\rm pyDOM}$ values in combina-

tion with its low metal contents (Table 1). We note that past studies on pyDOM redox properties exclusively reported EAC and EDC values and did not assess active participation of pyDOM in redox reactions through monitoring changes in the redox state of pyDOM during the reactions.

Enzymatic Oxidation of pyDOM. We treated pyDOM_{G400} by a laccase from T. versicolor. Laccases are important phenol oxidases that largely contribute to the oxidative degradation of (dissolved) organic matter in oxic environments. 40,46,53,54 We herein aimed to directly demonstrate that the laccase was capable of oxidizing phenolic moieties in pyDOM. Incubation of pyDOM_{G400} with laccase indeed resulted in a pronounced decrease in EDC_{pyDOM} values within the first hour of laccase incubation (from 2.3 to 1.2 $\text{mmol}_{e^-} \cdot g_C^{-1}$) (Figure 4A). Because NPOC values remained constant, decreases in EDC_{pvDOM} solely reflect decreases in EDC_{pvDOM}. The $EDC_{pyDOM}^{r,r}$ continued to decrease over the remaining incubation time and leveled off at a value of 0.73 mmol_e- ${\rm g_C}^{-1}$ after 48 h. No decrease in the EDC $_{\rm pyDOM}$ was observed in laccase-free controls (Figure 4A) over the same incubation time. As the EDC_{pyDOM} decreased over the course of the incubation, the EAC_{pyDOM} increased (i.e., from 0.68 to 0.93 $mmol_{e-}g_C^{-1}$). However, this increase was much smaller (i.e., $0.26 \text{ mmol}_{e^-} \cdot g_C^{-1}$) than the corresponding decrease in EDC_{pyDOM} (i.e., 1.60 mmol_e- $\cdot g_C^{-1}$), implying that the majority of electron-donating moieties in the pyDOM accessible to laccase were irreversibly oxidized (i.e., oxidation did not result in an equimolar conversion of electron-donating to electronaccepting moieties). These findings are consistent with the irreversible oxidation of mono-hydroxylated (i.e., "phenolic") and meta-dihydroxylated aromatic moieties in the pyDOM, while the small increase in EAC_{pyDOM} may suggest the reversible oxidation of hydroquinone to the corresponding electron-accepting quinone moieties. This data demonstrates the enzymatic oxidizability of electron-donating moieties in pyDOM, suggesting that pyDOM is susceptible to enzymatic oxidation in the environment. We note that we did not test the solution for dissolved H₂O₂ (nor other partially reduced oxygen species) because laccases are known to completely reduce the co-substrate oxygen to water in a four-electron transfer reaction.

Reduction of pyDOM. In the second experiment, we assessed the reducibility of electron-accepting moieties in pyDOM_{G400}. To this end, we used non-mediated electrochemical reduction in an electrochemical cell at $E_h = -0.47 \text{ V}$ and pH 7 for 24 h (see the Materials and Methods section). We previously showed for DOM that such electrochemical reduction transfers electrons to the same electron-accepting moieties that are used by anaerobic microorganisms that use DOM as terminal electron acceptor. 55 The reduction of pyDOM at the working electrode would therefore strongly support that pyDOM may also act as a terminal electron acceptor in anaerobic microbial respiration. Over the course of the experiment (Figure 4B), the EAC_{pyDOM} of pyDOM_{G400} decreased from 0.62 to 0.38 mmol_e–·g_C⁻¹ while the EDC_{pyDOM} increased from 2.53 to 2.70 mmol_e–·g_C⁻¹. These finding demonstrate that pyDOM_{G400} was reducible and that its reduction was largely reversible (i.e., the increase in EDC_{pyDOM} of 0.17 mmol_e- g_C^{-1} corresponded to 84% of the EAC_{pyDOM} decrease of 0.24 mmol_e-g_C⁻¹). This finding is fully consistent with electron transfer to quinones in pyDOM_{G400} under the formation of the corresponding hydroquinones that contribute to EDC. We note that both Fe and Mn concentrations were

negligible relative to the EEC_{pyDOM} of this sample (Table 1), and thus did not contribute to the observed reversible reduction. Overall, our data suggest that pyDOM will be an environmentally relevant electron acceptor under reducing conditions.

Implications. All pyDOM specimens evaluated herein are redox-active regardless of the pyrolysis temperature and feedstock. Furthermore, pyDOM contain a larger number of redox-active moieties on a per gram carbon basis than the bulk chars from which they are derived. These findings suggest that pyDOM is an important redox-active phase in the environment and needs to be considered in biogeochemical redox cycles and pollutant redox transformations, particularly in environments impacted by pyrogenic organic matter. The importance of pyDOM in such redox reactions is expected to increase in the future, given that the frequency, extent, and severity of wildfires have largely increased globally over the last years. 56,57 We note that pyDOM entering the aquatic environment may not only alter redox equilibria in these systems but also cause new challenges if these systems serve as drinking water sources. Increasing concentrations of pyDOM in such water sources may demand increasing chemical oxidant doses for water disinfection while, at the same time, increasing the risk of toxic disinfection byproducts formation upon reaction between the chemical oxidants and pyDOM. While we demonstrated that pyDOM is redox-active and participates in biogeochemically important redox reactions, future work is needed to elucidate the release dynamics of pyDOM from chars formed in the open environment and how the chemical composition of the released pyDOM and its redox properties may change over

Consistent with previous work on non-pyrogenic DOM, the redox properties of the pyDOM are consistent with phenols and quinones as major electron-donating and -accepting organic moieties. Yet, for pyDOM from high-temperature wood chars, contributions of Mn and possibly char nanoparticles to redox capacities need careful consideration. Our findings suggest that both the quantity and redox properties of pyDOM reflect the physicochemical properties of the corresponding chars. While the importance of chars in mediating redox reactions relevant to pollutant dynamics and biogeochemical processes has been demonstrated, our work paves the way for systematic assessments of the role of pyDOM in these reactions. Our work supports that pyDOM acts both as an electron transfer mediator and hence redox catalyst and as a redox buffer that reversibly accepts electrons under reducing conditions and is irreversibly oxidized under oxidizing conditions.

ASSOCIATED CONTENT

Supporting Information

The Supporting Information is available free of charge at https://pubs.acs.org/doi/10.1021/acs.est.1c02429.

Chemicals; selected physicochemical properties of the 14 analyzed char specimens; electron-accepting capacity (EAC) and electron-donating capacity (EDC) values of 14 types of chars and pyDOM extracts from these chars; dissolved carbon as a fraction of total char carbon; absorbance ratios at 250 nm over 365 nm for pyDOM extracts from 14 types of chars; specific ultraviolet absorbance values of pyDOM extracts from grass and wood chars plotted vs. the calculated double-bond

equivalents (DBE) of the corresponding source chars from which pyDOM was extracted; and backgroundcorrected oxidative and reductive current responses on the flow-injection analysis (FIA) system for standard solutions of (A) 1, 5, 10, and 20 μ mol L⁻¹ of ascorbate and one blank sample and of (B) 1, 5, 10, and 20 μ mol L⁻¹ of 2,6-AQDS and one blank sample (PDF).

AUTHOR INFORMATION

Corresponding Author

Wenqing Xu - Department of Civil and Environmental Engineering, Villanova University, Villanova, Pennsylvania 19085, United States; orcid.org/0000-0002-9838-8220; Phone: 001-(610) 519-8549; Email: wenqing.xu@ villanova.edu

Authors

Nicolas Walpen - Institute of Biogeochemistry and Pollutant Dynamics, ETH Zurich, 8092 Zurich, Switzerland; orcid.org/0000-0002-7177-5175

Marco Keiluweit - School of Earth & Sustainability and Stockbridge School of Agriculture, University of Massachusetts Amherst, Amherst, Massachusetts 01003, United States; orcid.org/0000-0002-7061-8346

Markus Kleber - Department of Crop and Soil Science, Oregon State University, Corvallis, Oregon 97331, United

Michael Sander – Institute of Biogeochemistry and Pollutant Dynamics, ETH Zurich, 8092 Zurich, Switzerland; orcid.org/0000-0003-3383-2041

Complete contact information is available at: https://pubs.acs.org/10.1021/acs.est.1c02429

Notes

The authors declare no competing financial interest.

ACKNOWLEDGMENTS

W.X. thanks Professor Kristopher McNeill at ETH Zurich for hosting her sabbatical, the U.S. National Science Foundation CAREER award (CBET-1752220), and the Strategic Environmental Research and Development Program (SERDP ER19-1239) under the U.S. Department of Defense for the financial support. N.W. and M.S. thank the Swiss National Science Foundation (Project 200020 159692) for funding and ETH Zurich for funding the FIA system via the Scientific Equipment Program. M. Keiluweit was supported through the U.S. Department of Energy (DE-SC0020205). The authors also thank Dr. Björn Studer at ETH Zurich for his help in measuring the concentrations of metals in pyDOM samples.

REFERENCES

- (1) Gustafsson, Ö.; Gschwend, P. M. The flux of black carbon to surface sediments on the New England continental shelf. Geochim. Cosmochim. Acta 1998, 62, 465-472.
- (2) Jonker, M. T.; Koelmans, A. A. Sorption of polycyclic aromatic hydrocarbons and polychlorinated biphenyls to soot and soot-like materials in the aqueous environment: mechanistic considerations. Environ. Sci. Technol. 2002, 36, 3725-3734.
- (3) Koelmans, A. A.; Jonker, M. T. O.; Cornelissen, G.; Bucheli, T. D.; Van Noort, P. C. M.; Gustafsson, O. Black carbon: The reverse of its dark side. Chemosphere 2006, 63, 365-377.
- (4) Masiello, C. A. New directions in black carbon organic geochemistry. Mar. Chem. 2004, 92, 201-213.

- (5) Middelburg, J. J.; Nieuwenhuize, J.; van Breugel, P. Black carbon in marine sediments. Mar. Chem. 1999, 65, 245-252.
- (6) Pignatello, J.; Mitch, W. A.; Xu, W. Activity and reactivity of pyrogenic carbonaceous matter toward organic compounds. Environ. Sci. Technol. 2017, 51, 8893-8908.
- (7) Cayuela, M.; Van Zwieten, L.; Singh, B.; Jeffery, S.; Roig, A.; Sánchez-Monedero, M. Biochar's role in mitigating soil nitrous oxide emissions: A review and meta-analysis. Agric., Ecosyst. Environ. 2014, 191, 5-16.
- (8) Chen, S. S.; Rotaru, A. E.; Shrestha, P. M.; Malvankar, N. S.; Liu, F. H.; Fan, W.; Nevin, K. P.; Lovley, D. R. Promoting Interspecies Electron Transfer with Biochar. Sci. Rep. 2014, 4, No. 5019.
- (9) Ding, K.; Byrnes, C.; Bridge, J.; Grannas, A.; Xu, W. Surfacepromoted hydrolysis of 2, 4, 6-trinitrotoluene and 2, 4-dinitroanisole on pyrogenic carbonaceous matter. Chemosphere 2018, 197, 603-610.
- (10) Ding, K.; Duran, M.; Xu, W. The synergistic interaction between sulfate-reducing bacteria and pyrogenic carbonaceous matter in DDT decay. Chemosphere 2019, 233, 252-260.
- (11) Ding, K.; Xu, W. Black Carbon Facilitated Dechlorination of DDT and its Metabolites by Sulfide. Environ. Sci. Technol. 2016, 50, 12976-12983.
- (12) Fu, H.; Zhu, D. Graphene oxide-facilitated reduction of nitrobenzene in sulfide-containing aqueous solutions. Environ. Sci. Technol. 2013, 47, 4204-4210.
- (13) Kappler, A.; Wuestner, M. L.; Ruecker, A.; Harter, J.; Halama, M.; Behrens, S. Biochar as an electron shuttle between bacteria and Fe (III) minerals. Environ. Sci. Technol. Lett. 2014, 1, 339-344.
- (14) Kemper, J. M.; Ammar, E.; Mitch, W. A. Abiotic degradation of hexahydro-1,3,5-trinitro-1,3,5-triazine in the presence of hydrogen sulfide and black carbon. Environ. Sci. Technol. 2008, 42, 2118-2123.
- (15) Klüpfel, L.; Keiluweit, M.; Kleber, M.; Sander, M. Redox properties of plant biomass-derived black carbon (biochar). Environ. Sci. Technol. 2014, 48, 5601-5611.
- (16) Liu, F. H.; Rotaru, A. E.; Shrestha, P. M.; Malvankar, N. S.; Nevin, K. P.; Lovley, D. R. Promoting direct interspecies electron transfer with activated carbon (vol 4, pg 8982, 2012). Energy Environ. Sci. 2013, 6, 3790-3791.
- (17) Oh, S. Y.; Chiu, P. C. Graphite- and Soot-Mediated Reduction of 2,4-Dinitrotoluene and Hexahydro-1,3,5-trinitro-1,3,5-triazine. Environ. Sci. Technol. 2009, 43, 6983-6988.
- (18) Oh, S. Y.; Son, J. G.; Chiu, P. C. Biochar-mediated reductive transformation of nitro herbicides and explosives. Environ. Toxicol. Chem. 2013, 32, 501-508.
- (19) Xu, S.; Adhikari, D.; Huang, R.; Zhang, H.; Tang, Y.; Roden, E.; Yang, Y. Biochar-facilitated microbial reduction of hematite. Environ. Sci. Technol. 2016, 50, 2389-2395.
- (20) Xu, W.; Pignatello, J. J.; Mitch, W. A. Role of black carbon electrical conductivity in mediating hexahydro-1, 3, 5-trinitro-1, 3, 5triazine (RDX) transformation on carbon surfaces by sulfides. Environ. Sci. Technol. 2013, 47, 7129-7136.
- (21) Xu, W.; Pignatello, J. J.; Mitch, W. A. Reduction of nitroaromatics sorbed to black carbon by direct reaction with sorbed sulfides. Environ. Sci. Technol. 2015, 49, 3419-3426.
- (22) Xu, W. Q.; Dana, K. E.; Mitch, W. A. Black Carbon-Mediated Destruction of Nitroglycerin and RDX By Hydrogen Sulfide. Environ. Sci. Technol. 2010, 44, 6409-6415.
- (23) Xu, W. S.; M, L.; Li, Z. Reactivity of Pyrogenic Carbonaceous Matter (PCM) in Mediating Environmental Reactions: Current Knowledge and Future Trends. Front. Environ. Sci. Eng. 2020, 14,
- (24) Xu, X.; Sivey, J. D.; Xu, W. Black carbon-enhanced transformation of dichloroacetamide safeners: Role of reduced sulfur species. Sci. Total Environ. 2020, 738, No. 139908.
- (25) Yang, J.; Pan, B.; Li, H.; Liao, S.; Zhang, D.; Wu, M.; Xing, B. Degradation of p-nitrophenol on biochars: role of persistent free radicals. Environ. Sci. Technol. 2016, 50, 694-700.
- (26) Xin, D.; Xian, M.; Chiu, P. C. New methods for assessing electron storage capacity and redox reversibility of biochar. Chemosphere 2019, 215, 827-834.

- (27) Sun, T. R.; Levin, B. D. A.; Guzman, J. J. L.; Enders, A.; Muller, D. A.; Angenent, L. T.; Lehmann, J. Rapid electron transfer by the carbon matrix in natural pyrogenic carbon. *Nat. Commun.* **2017**, *8*, No. 14873.
- (28) Harter, J.; Krause, H.-M.; Schuettler, S.; Ruser, R.; Fromme, M.; Scholten, T.; Kappler, A.; Behrens, S. Linking N2O emissions from biochar-amended soil to the structure and function of the N-cycling microbial community. *ISME J.* **2014**, *8*, 660–674.
- (29) Payne, R. B.; Ghosh, U.; May, H. D.; Marshall, C. W.; Sowers, K. R. A Pilot-Scale Field Study: In Situ Treatment of PCB-Impacted Sediments with Bioamended Activated Carbon. *Environ. Sci. Technol.* **2019**, 53, 2626–2634.
- (30) Kjellerup, B.; Naff, C.; Edwards, S.; Ghosh, U.; Baker, J.; Sowers, K. Effects of activated carbon on reductive dechlorination of PCBs by organohalide respiring bacteria indigenous to sediments. *Water Res.* **2014**, *52*, 1–10.
- (31) Lefèvre, E.; Bossa, N.; Gardner, C. M.; Gehrke, G. E.; Cooper, E. M.; Stapleton, H. M.; Hsu-Kim, H.; Gunsch, C. K. Biochar and activated carbon act as promising amendments for promoting the microbial debromination of tetrabromobisphenol A. *Water Res.* **2018**, *128*, 102–110.
- (32) Saquing, J. M.; Yu, Y.-H.; Chiu, P. C. Wood-derived black carbon (biochar) as a microbial electron donor and acceptor. *Environ. Sci. Technol. Lett.* **2016**, *3*, 62–66.
- (33) Zhang, B.; Zhou, S.; Zhou, L.; Wen, J.; Yuan, Y. Pyrolysis temperature-dependent electron transfer capacities of dissolved organic matters derived from wheat straw biochar. *Sci. Total Environ.* **2019**, *696*, No. 133895.
- (34) Zheng, X.; Liu, Y.; Fu, H.; Qu, X.; Yan, M.; Zhang, S.; Zhu, D. Comparing electron donating/accepting capacities (EDC/EAC) between crop residue-derived dissolved black carbon and standard humic substances. *Sci. Total Environ.* **2019**, *673*, 29–35.
- (35) Thurman, E. M. Organic Geochemistry of Natural Waters; Springer Science & Business Media, 2012; Vol. 2.
- (36) Bird, M. I.; Wynn, J. G.; Saiz, G.; Wurster, C. M.; McBeath, A. The pyrogenic carbon cycle. *Annu. Rev. Earth Planet. Sci.* **2015**, 43, 273–298.
- (37) Dittmar, T.; De Rezende, C. E.; Manecki, M.; Niggemann, J.; Ovalle, A. R. C.; Stubbins, A.; Bernardes, M. C. Continuous flux of dissolved black carbon from a vanished tropical forest biome. *Nat. Geosci.* **2012**, *5*, 618–622.
- (38) Keiluweit, M.; Nico, P. S.; Johnson, M. G.; Kleber, M. Dynamic molecular structure of plant biomass-derived black carbon (biochar). *Environ. Sci. Technol.* **2010**, *44*, 1247–1253.
- (39) Walpen, N.; Getzinger, G. J.; Schroth, M. H.; Sander, M. Electron-donating phenolic and electron-accepting quinone moieties in peat dissolved organic matter: quantities and redox transformations in the context of peat biogeochemistry. *Environ. Sci. Technol.* **2018**, 52,5236–5345
- (40) Walpen, N.; Schroth, M. H.; Sander, M. Quantification of phenolic antioxidant moieties in dissolved organic matter by flow-injection analysis with electrochemical detection. *Environ. Sci. Technol.* **2016**, *50*, 6423–6432.
- (41) Hammes, K.; Smernik, R. J.; Skjemstad, J. O.; Herzog, A.; Vogt, U. F.; Schmidt, M. W. Synthesis and characterisation of laboratory-charred grass straw (*Oryza sativa*) and chestnut wood (*Castanea sativa*) as reference materials for black carbon quantification. *Org. Geochem.* **2006**, *37*, 1629–1633.
- (42) Liu, C.-H.; Chu, W.; Li, H.; Boyd, S. A.; Teppen, B. J.; Mao, J.; Lehmann, J.; Zhang, W. Quantification and characterization of dissolved organic carbon from biochars. *Geoderma* **2019**, 335, 161–169
- (43) Uchimiya, M.; Ohno, T.; He, Z. Pyrolysis temperature-dependent release of dissolved organic carbon from plant, manure, and biorefinery wastes. *J. Anal. Appl. Pyrolysis* **2013**, *104*, 84–94.
- (44) Kleber, M.; Hockaday, W.; Nico, P. S. Characteristics of Biochar: Macro-Molecular Properties. In *Biochar for Environmental Management: Science, Technology and Implementation*, Routledge: Oxfordshire, 2015; pp 111–137.

- (45) Matilainen, A.; Gjessing, E. T.; Lahtinen, T.; Hed, L.; Bhatnagar, A.; Sillanpää, M. An overview of the methods used in the characterisation of natural organic matter (NOM) in relation to drinking water treatment. *Chemosphere* **2011**, 83, 1431–1442.
- (46) Thurston, C. F. The structure and function of fungal laccases. *Microbiology* **1994**, *140*, 19–26.
- (47) Weishaar, J. L.; Aiken, G. R.; Bergamaschi, B. A.; Fram, M. S.; Fujii, R.; Mopper, K. Evaluation of specific ultraviolet absorbance as an indicator of the chemical composition and reactivity of dissolved organic carbon. *Environ. Sci. Technol.* **2003**, *37*, 4702–4708.
- (48) De Haan, H.; De Boer, T. Applicability of light absorbance and fluorescence as measures of concentration and molecular size of dissolved organic carbon in humic Lake Tjeukemeer. *Water Res.* **1987**, 21, 731–734.
- (49) Zhao, X.; Zhang, L.; Liu, D. Biomass recalcitrance. Part I: the chemical compositions and physical structures affecting the enzymatic hydrolysis of lignocellulose. *Biofuels, Bioprod. Biorefin.* **2012**, *6*, 465–482.
- (50) Nimz, H.; Robert, D.; Faix, O.; Nemr, M. Carbon-13 NMR spectra of lignins, 8. Structural differences between lignins of hardwoods, softwoods, grasses and compression wood. *Holzforschung* **1981**, 35, 16–26.
- (51) Yang, H.; Yan, R.; Chen, H.; Lee, D. H.; Zheng, C. Characteristics of hemicellulose, cellulose and lignin pyrolysis. *Fuel* **2007**, *86*, 1781–1788.
- (52) Mayer, A.; Gorham, E. The iron and manganese content of plants present in the natural vegetation of the English Lake District. *Ann. Bot.* **1951**, *15*, 247–263.
- (53) Aeschbacher, M.; Graf, C.; Schwarzenbach, R. P.; Sander, M. Antioxidant Properties of Humic Substances. *Environ. Sci. Technol.* **2012**, *46*, 4916–4925.
- (54) Baldrian, P. Fungal laccases—occurrence and properties. *FEMS Microbiol. Rev.* **2006**, *30*, 215–242.
- (55) Klüpfel, L.; Piepenbrock, A.; Kappler, A.; Sander, M. Humic substances as fully regenerable electron acceptors in recurrently anoxic environments. *Nat. Geosci.* **2014**, *7*, 195–200.
- (56) Smith, H. G.; Sheridan, G. J.; Lane, P. N.; Nyman, P.; Haydon, S. Wildfire effects on water quality in forest catchments: a review with implications for water supply. *J. Hydrol.* **2011**, 396, 170–192.
- (57) Hohner, A. K.; Rhoades, C. C.; Wilkerson, P.; Rosario-Ortiz, F. L. Wildfires alter forest watersheds and threaten drinking water quality. *Acc. Chem. Res.* **2019**, *52*, 1234–1244.